Technobius Physics, 2024, 2(3), 0016, DOI: https://doi.org/10.54355/tbusphys/2.3.2024.0016

Technobius Physics

https://technobiusphysics.kz/

e-ISSN 3007-0147

Corrigendum Notice: A corrigendum has been issued for this article and is included at the end of this document.

Article

Determining magnetic field strength as a function of current in Helmholtz coils

Nazerke Erzhanova*

Astana International University, School of Natural Sciences, 8 Kabanbay ave., Astana, Kazakhstan
*Correspondence: nazerke.erzhanova@internet.ru

Abstract. This study investigates the correlation between the magnetic field strength generated by two Helmholtz coils and the current passing through them. Utilizing a 100 Ohm, 1.8 A rheostat, the Helmholtz coils are connected to a variable power source (0-20V, 0-5A), ensuring stable positioning. The magnetic field at the center of the coils is precisely measured using a digital Teslameter with a Hall probe, as the current is incrementally adjusted. A digital multimeter, equipped with multiple operational modes, facilitates data collection and ensures accuracy. The empirical validation of theoretical predictions is achieved by plotting magnetic field strength against current. Adherence to stringent safety protocols, such as temperature monitoring and secure electrical connections, is maintained throughout the experiment. Helmholtz coils are mounted on a robust core assembly using supports, clamps, and rods to ensure alignment and stability. The experimental setup includes the calculation of the calibration factor and the horizontal flux density as a function of coil current. Additionally, the maximum needle deflection at 4 A allows for the measurement of the angle between the coil axis and the "north/south" direction.

Keywords: Helmholtz coils, magnetic field strength, current variation, digital teslameter, calibration factor.

1. Introduction

The magnetic field of Earth is an important component of the geophysical environment of the planet and has been studied by scientists for many years. This magnetic field, which is derived from the dynamo action in the fluid outer core of the Earth, has a significant impact on a number of natural and manmade processes. Geodynamics, tectonics, and the Earth's evolutionary history are all greatly aided by an understanding of the origin, structure, and dynamic changes of the geomagnetic field. By using satellite missions and ground-based observatories, exact measurements and analysis are used to reach this full understanding [1], [2], [3].

The geodynamo, or motion of molten iron and nickel in the outer core, is the primary source of the Earth's magnetic field [4]. Convection currents generated by the heat created by the radioactive decay of materials within the Earth are what propel this dynamo action [5]. With magnetic poles close to the geographic poles, the resulting magnetic field is mostly dipolar. However, because of the dynamic nature of the geodynamo process, the field also displays intricate non-dipolar components that change over time [6], [7].

Long-term, continuous records of the Earth's magnetic field have been made possible thanks in large part to ground-based magnetic observatories. These observatories use fluxgate magnetometers and proton precession magnetometers to measure the three components of the geomagnetic field: intensity, inclination, and declination. These data are essential for tracking secular variations, spotting magnetic abnormalities, and researching unusual events such abrupt shifts in the secular variation's rate, or geomagnetic jerks [8], [9].

Utilizing cutting-edge technologies and approaches, recent studies of the Earth's magnetic field have improved our comprehension of this intricate geophysical phenomenon. Improved modeling methods, high-resolution observations, and the local and global effects of magnetic field fluctuations have been the main topics of these investigations [10], [11].

The use of high-resolution satellite missions has been one of the most important developments in the study of the Earth's magnetic field. Launched in 2013, the European Space Agency's Swarm mission consists of three identical satellites operating in a constellation to monitor magnetic signals with previously unheard-of accuracy from the Earth's core, mantle, crust, oceans, ionosphere, and magnetosphere [12], [13]. Swarm data have given deep insights into core-mantle interactions, the dynamics of the geodynamo, and the impact of external sources like solar activity on the geomagnetic field. Researchers may now examine the fine-scale characteristics of the Earth's magnetic field and develop more precise global geomagnetic models thanks to the Swarm mission. For instance, complex structures of magnetic anomalies and secular fluctuation have been discovered by recent analysis of Swarm data, which has improved our comprehension of the underlying geodynamic processes. Furthermore, studying geomagnetic jerks—rapid variations in the geomagnetic field—and their consequences for the mechanics of the Earth's core have been made possible thanks in large part to Swarm data [13].

With the availability of high-resolution data, research on abrupt variations in the Earth's magnetic field, or geomagnetic jerks, has advanced dramatically. Studying geomagnetic jerks, which are abrupt increases in the rate of secular fluctuation, can provide important details about the inner workings of the Earth. The goal of recent studies has been to determine the cause of these jerks and how core-mantle interactions relate to them. For instance, a study that discovered a geomagnetic jerk that happened in 2015 using Swarm data shed light on the underlying mechanics. The results imply that these quick changes could be related to modifications in the flow patterns caused by compositional and thermal convection processes in the Earth's outer core [14], [15].

Thanks to recent developments, the useful applications of geomagnetic field investigations are growing. Improved geomagnetic models improve GPS and compass accuracy, which is important for aerial and marine navigation. Extensive magnetic surveys are used in mineral exploration to find subsurface mineral deposits, which benefits the mining sector [16].

In this paper, to better understand the properties of magnetic fields, two kinds of Helmholtz coils, round and square, of equal size, have been used.

2. Methods

This experiment looks at the relationship between the current flowing through two Helmholtz coils and the strength of the magnetic field they produce. To control current flow, the Helmholtz coils are firmly installed and linked to a variable power source with 0-20V and 0-5 A via a rheostat of 100 Ohm and 1.8 A. As the current is gradually changed, the magnetic field at the coils' center is precisely measured using a digital Teslameter fitted with a Hall probe. A digital multimeter in operating mode of 600V AC/DC, 10A AC/DC, 20 MΩ, 200 μF, 20 kHz, −20°C – 760°C makes data collecting easier and ensures dependability by taking several readings.

By constructing a graph that plots magnetic field strength versus current using the obtained data, theoretical predictions are empirically validated. Strict safety precautions are followed during the experiment, such as keeping an eye on the temperatures of the equipment and making sure the electrical connections are secure to guarantee precise and safe measurements.

Using the proper stands, clamps, and rods with 250 mm of length and diameter of 10 mm , the Helmholtz coils are firmly fixed to a sturdy core assembly to guarantee alignment and stability during the experiment.

The rheostat and the multimeter that is used as an ammeter are used to connect the Helmholtz coils, along with the installed space holders, to the DC generator in series (a linkage of equally-

numbered connections). The barrel base of the Hall probe should point inward toward the coil axis in the middle of the Helmholtz arrangement when it is placed on the support rod (Figure 1).

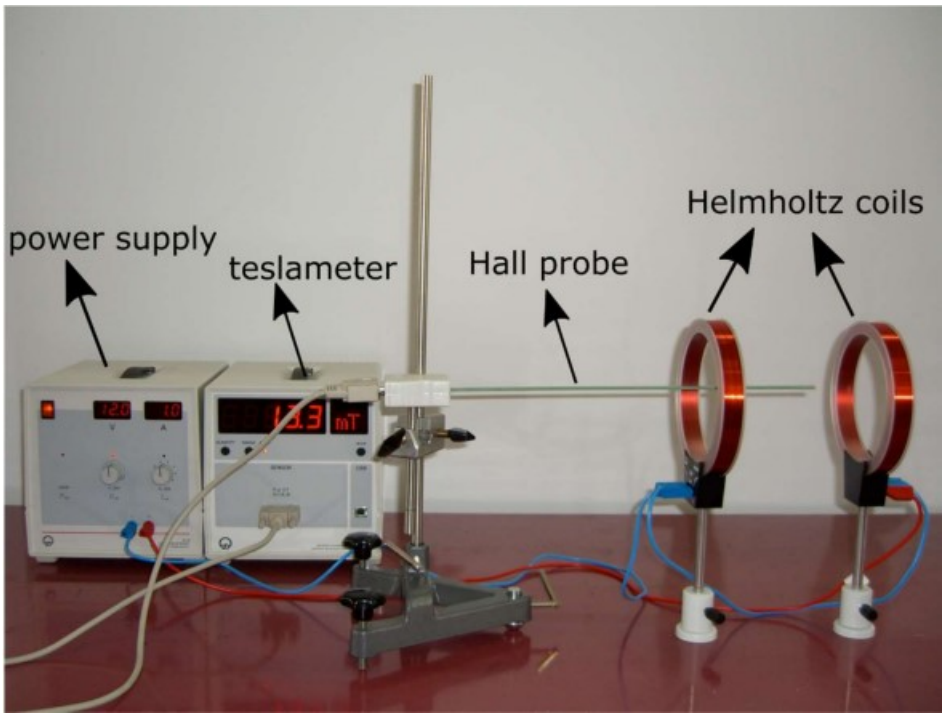

Figure 1 – Experimental equipment

The magnetometer's graded circle was then turned into the vertical plane while the coils were devoid of electricity, enabling the magnetic needle to display the inclination angle υ_1. The spin axis was carefully positioned to match the "north/south" direction accurately. The magnetometer was turned 180 degrees and reinstalled in the vertical plane to confirm υ_2.

The Teslameter's zero-point position was carefully calibrated prior to the measurements starting. The magnetometer, which had a leveled graduated circle, was being positioned between the coils using a barrel base, stand tube, and visual judgment to have the center of the graduated circle roughly aligned with the center of each pair of coils. Originally, when there was no current running through the coils, the direction "north/south" was marked on the graded circle. The magnetic needle was being gently deflected from its resting position many times to verify precise orientation, and the instrument was being carefully tapped to reduce friction resistance.

By measuring the deflection angle of the magnetic needle from its resting position in response to tiny currents given to the coils, the horizontal component of the Earth's magnetic field was found. The measurement series needed to be rerun if the coil current's polarity was switched. Readings from both ends of the needle were being considered in order to determine the exact angle.

To ensure the stability and precision of measurements, Helmholtz coils were fixed using rods (250 mm length, 10 mm diameter), clamps, and a rigid core base. The Teslameter's zero was calibrated prior to the experiment. The probe was placed at the geometric center between the coils to align with the axis. A magnetometer was used to determine the inclination and deflection of the magnetic needle, allowing calculation of the horizontal component of Earth's magnetic field.

The current through the coils was varied incrementally, and the magnetic field was measured at each step. For each current level, three repeated measurements of the magnetic field were taken to account for random fluctuations and ensure reliability. The measured values were used to compute:

– Arithmetic mean *M* of the magnetic field values:

$$M = \frac{1}{n}\sum_{i=1}^{n} x_i \quad (1)$$

– Standard deviation σ, which quantifies the spread of the data:

$$\sigma = \sqrt{\frac{1}{n-1}\sum_{i=1}^{n}(x_i - M)^2} \quad (2)$$

Where: n — number of measurements (here, n = 3); x_i — individual measured values; M — mean value. These statistics were used to estimate measurement uncertainty and plotted error bars in the graph of magnetic field vs. current. The relative error (%) was additionally calculated as:

$$\text{Relative error} = \left(\frac{\sigma}{M}\right) \cdot 100\% \quad (3)$$

The consistency of experimental values with theoretical predictions was evaluated by plotting the magnetic field strength versus current and analyzing the linearity. Deviations from the theoretical model were assessed based on the calculated error margins. This allowed validation of the experiment and identification of potential systematic errors.

Strict safety protocols were observed, including temperature control and secure electrical connections, to ensure both measurement integrity and safe operating conditions throughout the experiment.

3. Results and Discussion

In this paper, for a better understanding of the properties of magnetic fields, they were generated by two kinds of Helmholtz coils, round and square of equal size. The geometric sizes of the two coil pairs are set to the same value: the side length of the square coil pair is 100 mm, and the radius of the circular coil pair is 50 mm, in order to analyze the magnetic fields of the two coil pairs.

According to the data, the magnetic field distribution on the Y-axis of the square and circular coils is displayed in Figure 3. From this, a sizable area of uniform magnetic field in both coils can be obtained. The horizontal flux density ${}^{h}B_H$ of the two coils in this setup must be calculated as a function of the coil current I_H. The accompanying graphic representation aids in the determination of the calibration factor $K = \frac{{}^{h}B_H}{I_H}$ (Figure 2). By short-circuiting the resistor, removing the ammeter, and setting the coil current to about 4 A, the maximum needle deflection was achieved. This allowed for the determination of the angle α (Figure 3) between the "north/south" direction and the axis of the two coils.

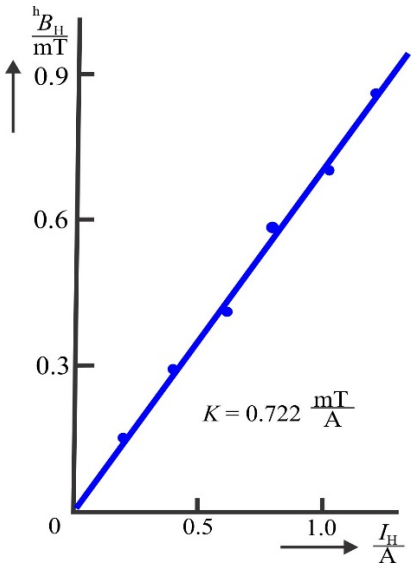

Figure 2 – Function of calibration for the two Helmholtz coils

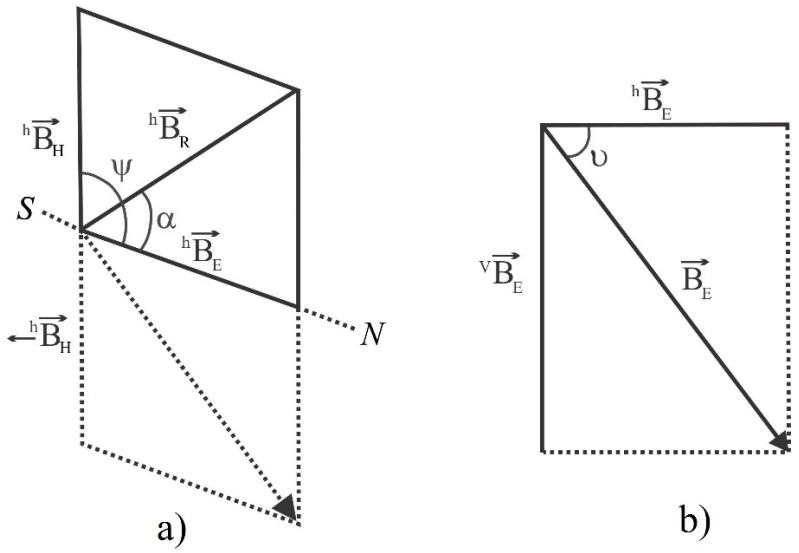

Figure 3 – The magnetic flux densities are shown as a vector graphic with: a) horizontal plane and b) vertical plane

It is possible to look at the connection between the measured values and the theoretical predictions. On Figure 4 the horizontal component of the Earth's magnetic field can be directly measured by the slope of this function, when $I_H * K$ is seen as a function of $\frac{sin\alpha}{sin\beta}$.

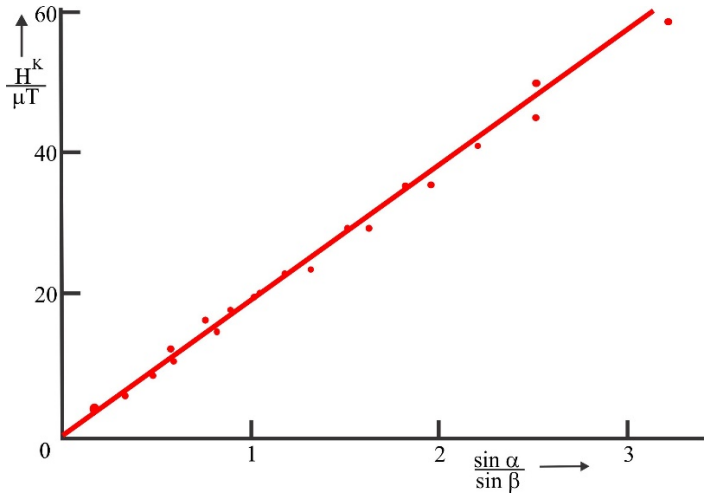

Figure 4 – Linear function of the Earth magnetic field's horizontal component of the magnetic flux density

This correlation shows that this component was successfully measured and captured by the experiment. Moreover, the measured angle of inclination and the vertical component of the Earth's magnetic field were inferred from the data shown (^hB_H = 18.8 mkT) according Figure 2b. The accuracy of our experimental setup and measurement procedures in defining both components of the Earth's magnetic field is validated by the consistency between the experimental results and theoretical expectations:

$$\upsilon = \frac{1}{2}(\upsilon_1 + \upsilon_2) = \frac{1}{2}(67^o + 68^o) = 67.5^o \quad (4)$$

$$B_E = B_E \tan \upsilon = 46.3\ \mu T \quad (5)$$

Combining the horizontal component B_h and vertical component B_v found in the experiment yields the total magnetic flux density. These components must be added vector-wise in the calculation, usually using the following equation:

$$|B_E| = \sqrt{(B_E vertical)^2 + (B_E horizontal)^2} = 50.2\ mkT \quad (6)$$

This calculation provides a comprehensive measure of the total magnetic flux density at the location of the experiment, considering both the horizontal orientation relative to the Earth's surface and the vertical orientation towards or away from the Earth. The accuracy of this calculation is essential for understanding the overall strength and orientation of the Earth's magnetic field in the vicinity of the experiment.

For applications that require constant magnetic fields, it is critical to optimize design and ensure field uniformity by comparing the magnetic field data of square and circular Helmholtz coils. Evaluating the errors associated with each coil shape provides insights into their precision and reliability, aiding in the selection of the appropriate configuration for specific needs in industrial processes. This comparative analysis also offers theoretical and practical insights into how different geometries affect magnetic fields, guiding future coil designs and contributing to the development of new technologies. Additionally, understanding the trade-offs between performance, manufacturing complexity, and cost can lead to more informed decisions in coil design and application.

The Table 1 presents the calculated magnetic field data for two different types of Helmholtz coils: circular and square. Measurements were taken at various distances from the center of the coil, with corresponding calculated magnetic field strengths and associated errors (in percentages).

Table 1 – Obtained data of different type of Helmholtz coils

	Circular Helmholtz coils		Square Helmholtz coils	
y, mm	Calculated data, uT	Error, %	Calculated data, uT	Error, %
0	35.98	0.752	32.52	0.992
5	35.95	0.751	32.53	0.991
10	35.92	0.761	32.57	1.001
15	35.68	0.776	32.41	1.005
20	35.11	0.891	32.12	1.012

For the circular Helmholtz coils, the calculated magnetic field strength at the center (y = 0 mm) is 35.98 μT with an error of 0.752%. As the distance increases, the calculated magnetic field slightly decreases, reaching 35.11 μT at y = 20 mm, with the error increasing to 0.891%.

For the square Helmholtz coils, the initial calculated magnetic field strength at the center is 32.52 μT with an error of 0.992%. Similar to the circular coils, the magnetic field strength decreases with distance, recording 32.12 μT at y = 20 mm, and the error increases to 1.012%.

These data demonstrate the variation in magnetic field strength and associated errors between the circular and square Helmholtz coils across different distances from the center.

4. Conclusions

In summary, this experiment effectively used accurate measuring techniques with a digital Teslameter and magnetometer to examine the properties of the magnetic field generated by two Helmholtz coils and the components of the Earth's magnetic field. We found connections that confirmed theoretical assumptions by measuring the magnetic field intensities ${}^{h}B_H$ = 18.8 mkT by vertical component that resulted from methodically adjusting the current through the coils. The geographical distribution and intensity of the magnetic field in our experimental setup were better understood by calculating the overall magnetic flux density and determining the horizontal and vertical components of the Earth's magnetic field, that was indicated $B_E = 50.2\ mkT$. These discoveries are important for applications in geophysics, navigation, and related domains and further our understanding of magnetic field interactions. To better understand Earth's magnetic field dynamics, future research might concentrate on improving measuring methods and investigating differences in magnetic field intensity across different geographical locations.

The comparative analysis of circular and square Helmholtz coils reveals notable differences in their magnetic field strengths and associated errors across various distances. For instance, at the center (y = 0 mm), the circular Helmholtz coils generate a magnetic field strength of 35.98 μT with an error of 0.752%, while the square Helmholtz coils produce 32.52 μT with an error of 0.992%. As the distance increases to 20 mm, the magnetic field strength for circular coils decreases to 35.11 μT with an error of 0.891%, and for square coils, it decreases to 32.12 μT with an error of 1.012%. These findings are essential for optimizing coil design to achieve uniform magnetic fields, ensuring high precision, and balancing cost and manufacturing complexity. By understanding these differences, more informed decisions can be made in selecting the appropriate coil geometry, enhancing the effectiveness and efficiency of applications in scientific research, medical imaging, and industrial processes.

References

[1] F. Donadini, M. Korte, and C. Constable, “Millennial variations of the geomagnetic field: From data recovery to field reconstruction,” *Space Sci. Rev.*, vol. 155, no. 1–4, pp. 219–246, Aug. 2010, doi: 10.1007/S11214-010-9662-Y/METRICS.

[2] M. Dumberry and C. C. Finlay, “Eastward and westward drift of the Earth’s magnetic field for the last three millennia,” *Earth Planet. Sci. Lett.*, vol. 254, no. 1–2, pp. 146–157, Feb. 2007, doi: 10.1016/J.EPSL.2006.11.026.

[3] M. Korte, C. Constable, F. Donadini, and R. Holme, “Reconstructing the Holocene geomagnetic field,” *Earth*

Planet. Sci. Lett., vol. 312, no. 3–4, pp. 497–505, Dec. 2011, doi: 10.1016/J.EPSL.2011.10.031.
[4] E. M. King and B. A. Buffett, "Flow speeds and length scales in geodynamo models: The role of viscosity," *Earth Planet. Sci. Lett.*, vol. 371–372, pp. 156–162, Jun. 2013, doi: 10.1016/J.EPSL.2013.04.001.
[5] M. Kono and P. H. Roberts, "Definition of the Rayleigh number for geodynamo simulation," *Phys. Earth Planet. Inter.*, vol. 128, no. 1–4, pp. 13–24, Dec. 2001, doi: 10.1016/S0031-9201(01)00274-6.
[6] M. Schrinner, D. Schmitt, R. Cameron, and P. Hoyng, "Saturation and time dependence of geodynamo models," *Geophys. J. Int.*, vol. 182, no. 2, pp. 675–681, Aug. 2010, doi: 10.1111/J.1365-246X.2010.04650.X/2/M_182-2-675-EQ016.JPEG.
[7] M. D. Menu, L. Petitdemange, and S. Galtier, "Magnetic effects on fields morphologies and reversals in geodynamo simulations," *Phys. Earth Planet. Inter.*, vol. 307, Oct. 2020, doi: 10.1016/j.pepi.2020.106542.
[8] N. Olsen *et al.*, "The Swarm satellite constellation application and research facility (SCARF) and Swarm data products," *Earth, Planets Sp.*, vol. 65, no. 11, pp. 1189–1200, Nov. 2013, doi: 10.5047/EPS.2013.07.001/TABLES/4.
[9] C. C. Finlay, N. Olsen, and L. Tøffner-Clausen, "DTU candidate field models for IGRF-12 and the CHAOS-5 geomagnetic field model International Geomagnetic Reference Field - The Twelfth generation," *Earth, Planets Sp.*, vol. 67, no. 1, pp. 1–17, Dec. 2015, doi: 10.1186/S40623-015-0274-3/FIGURES/11.
[10] J. Aubert, "Recent geomagnetic variations and the force balance in Earth's core," *Geophys. J. Int.*, vol. 221, no. 1, pp. 378–393, Apr. 2020, doi: 10.1093/GJI/GGAA007.
[11] C. J. Davies, R. K. Bono, D. G. Meduri, J. Aubert, S. Greenwood, and A. J. Biggin, "Dynamo constraints on the long-term evolution of Earth's magnetic field strength," *Geophys. J. Int.*, vol. 228, no. 1, pp. 316–336, Sep. 2021, doi: 10.1093/GJI/GGAB342.
[12] G. Hulot *et al.*, "Swarm's absolute magnetometer experimental vector mode, an innovative capability for space magnetometry," *Geophys. Res. Lett.*, vol. 42, no. 5, pp. 1352–1359, Mar. 2015, doi: 10.1002/2014GL062700.
[13] R. Tozzi, M. Pezzopane, P. De Michelis, and M. Piersanti, "Applying a curl-B technique to Swarm vector data to estimate nighttime F region current intensities," *Geophys. Res. Lett.*, vol. 42, no. 15, pp. 6162–6169, Aug. 2015, doi: 10.1002/2015GL064841.
[14] S. Maus, "Mysterious misalignments between geomagnetic and stellar reference frames seen in CHAMP and Swarm satellite measurements," *Geophys. J. Int.*, vol. 203, no. 3, pp. 1873–1876, Dec. 2015, doi: 10.1093/GJI/GGV409.
[15] Q. Li *et al.*, "Performance Analysis of GPS/BDS Broadcast Ionospheric Models in Standard Point Positioning during 2021 Strong Geomagnetic Storms," *Remote Sens. 2022, Vol. 14, Page 4424*, vol. 14, no. 17, p. 4424, Sep. 2022, doi: 10.3390/RS14174424.
[16] X. Li, H. Cai, D. Li, C. Geng, L. Chen, and J. Xu, "Analysis of the influence of geomagnetic storms on the ionospheric model of beidou/GPS system," *Lect. Notes Electr. Eng.*, vol. 388, pp. 503–510, 2016, doi: 10.1007/978-981-10-0934-1_43/FIGURES/4.

Information about authors:
Nazerke Erzhanova – Master Student, School of Natural Science, Astana International University, 8 Kabanbay ave., Astana, Kazakhstan, nazerke.erzhanova@internet.ru

Author Contributions:
Nazerke Erzhanova – concept, methodology, resources, data collection, testing, modeling, analysis, visualization, interpretation, drafting, editing, funding acquisition.

Received: 03.06.2024
Revised: 25.07.2024
Accepted: 27.07.2024
Published: 29.07.2024

Conflict of Interest: The authors declare no conflict of interest.

Use of Artificial Intelligence (AI): The authors declare that AI was not used.

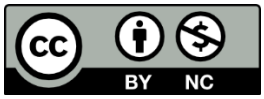

Copyright: @ 2024 by the authors. Licensee Technobius, LLP, Astana, Republic of Kazakhstan. This article is an open access article distributed under the terms and conditions of the Creative Commons Attribution (CC BY-NC 4.0) license (https://creativecommons.org/licenses/by-nc/4.0/).

Technobius Physics, 2024, 2(3), 0016c, DOI: https://doi.org/10.54355/tbusphys/2.3.2024.0016c

Technobius Physics

https://technobiusphysics.kz/

e-ISSN 3007-0147

Corrigendum Notice: A corrigendum has been issued for this article and is included at the end of this document.

Post-Publication Notice

Corrigendum to "N. Erzhanova, "Determining magnetic field strength as a function of current in Helmholtz coils", tbusphys, vol. 2, no. 3, p. 0016, Jul. 2024. doi: 10.54355/tbusphys/2.3.2024.0016"

In the originally published version of this article, the Methods section did not include details on the statistical processing of measurements and uncertainty estimation procedures. The following corrections have been made:

1. Section 2 (Methods):

- The updated version specifies repeated measurements (n=3) at each current level, calculation of arithmetic mean, standard deviation (σ), and relative error (%) for each data point.

- Error bars were added to the plotted graph of magnetic field versus current to visually represent measurement uncertainty.

- The consistency of experimental data with theoretical predictions was assessed based on these error estimates.

2. Editorial improvements were made to enhance the clarity of experimental descriptions and reliability of results.

These corrections do not alter the findings, discussion, or conclusions of the article but improve methodological transparency

Published: 13.08.2024

Copyright: @ 2024 by the authors. Licensee Technobius, LLP, Astana, Republic of Kazakhstan. This article is an open access article distributed under the terms and conditions of the Creative Commons Attribution (CC BY-NC 4.0) license (https://creativecommons.org/licenses/by-nc/4.0/).